Accurate Measurement of Residual Dipolar Couplings in Large RNAs by Variable Flip Angle NMR

Jan Marchant,[†,*] Ad Bax,[§] and Michael F. Summers[†,‡,*]

[†]Department of Chemistry and Biochemistry and [‡]Howard Hughes Medical Institute, University of Maryland Baltimore County (UMBC), Baltimore, MD 21250, [§]Laboratory of Chemical Physics, National Institute of Diabetes, Digestive and Kidney Diseases, National Institutes of Health, Bethesda MD 20892

janm@umbc.edu
bax@nih.gov
summers@hhmi.umbc.edu

Supporting Information

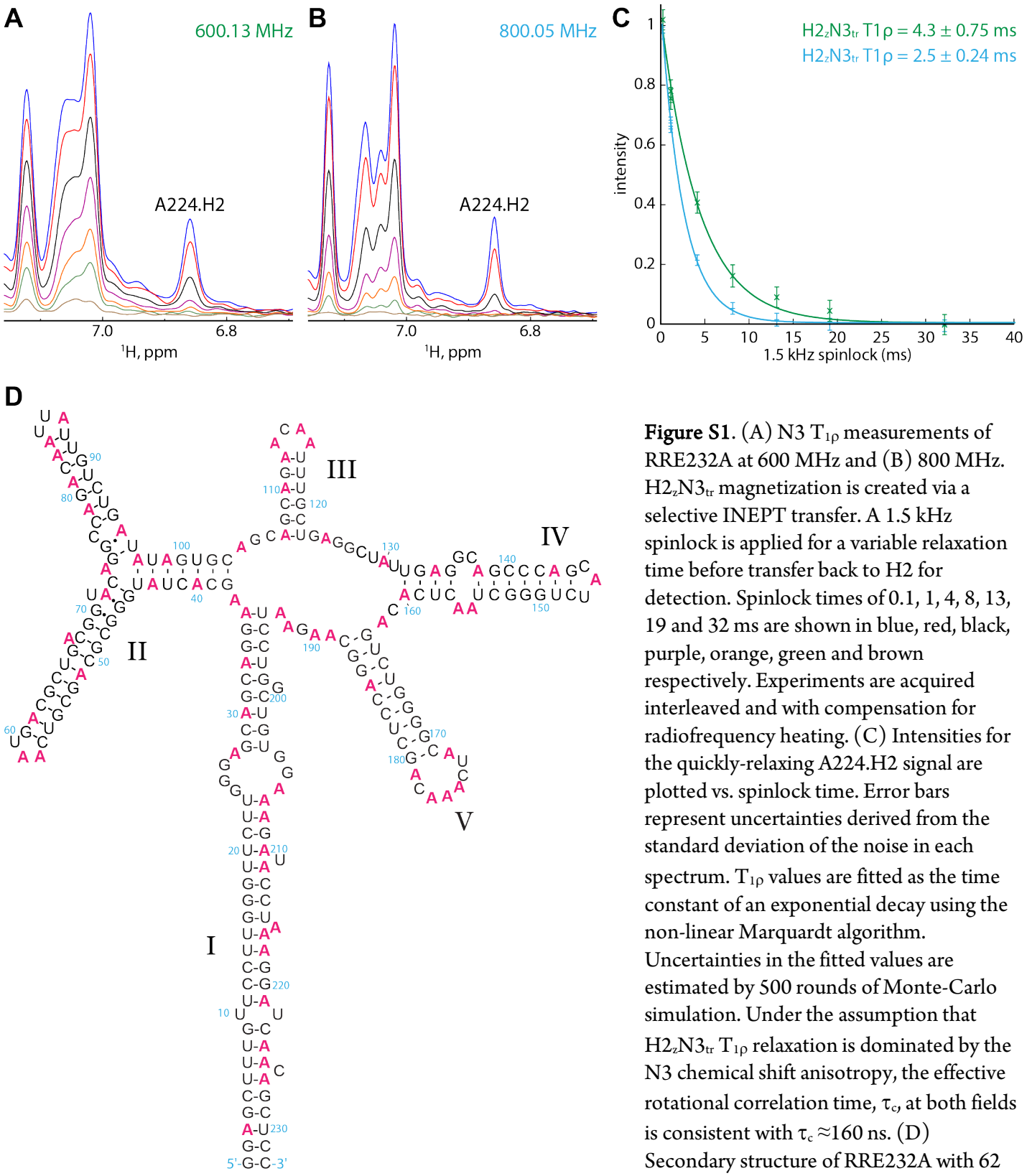

Figure S1. (A) N3 $T_{1\rho}$ measurements of RRE232A at 600 MHz and (B) 800 MHz. $H2_zN3_{tr}$ magnetization is created via a selective INEPT transfer. A 1.5 kHz spinlock is applied for a variable relaxation time before transfer back to H2 for detection. Spinlock times of 0.1, 1, 4, 8, 13, 19 and 32 ms are shown in blue, red, black, purple, orange, green and brown respectively. Experiments are acquired interleaved and with compensation for radiofrequency heating. (C) Intensities for the quickly-relaxing A224.H2 signal are plotted vs. spinlock time. Error bars represent uncertainties derived from the standard deviation of the noise in each spectrum. $T_{1\rho}$ values are fitted as the time constant of an exponential decay using the non-linear Marquardt algorithm. Uncertainties in the fitted values are estimated by 500 rounds of Monte-Carlo simulation. Under the assumption that $H2_zN3_{tr}$ $T_{1\rho}$ relaxation is dominated by the N3 chemical shift anisotropy, the effective rotational correlation time, τ_c, at both fields is consistent with $\tau_c \approx 160$ ns. (D) Secondary structure of RRE232A with 62 adenosines highlighted in pink.

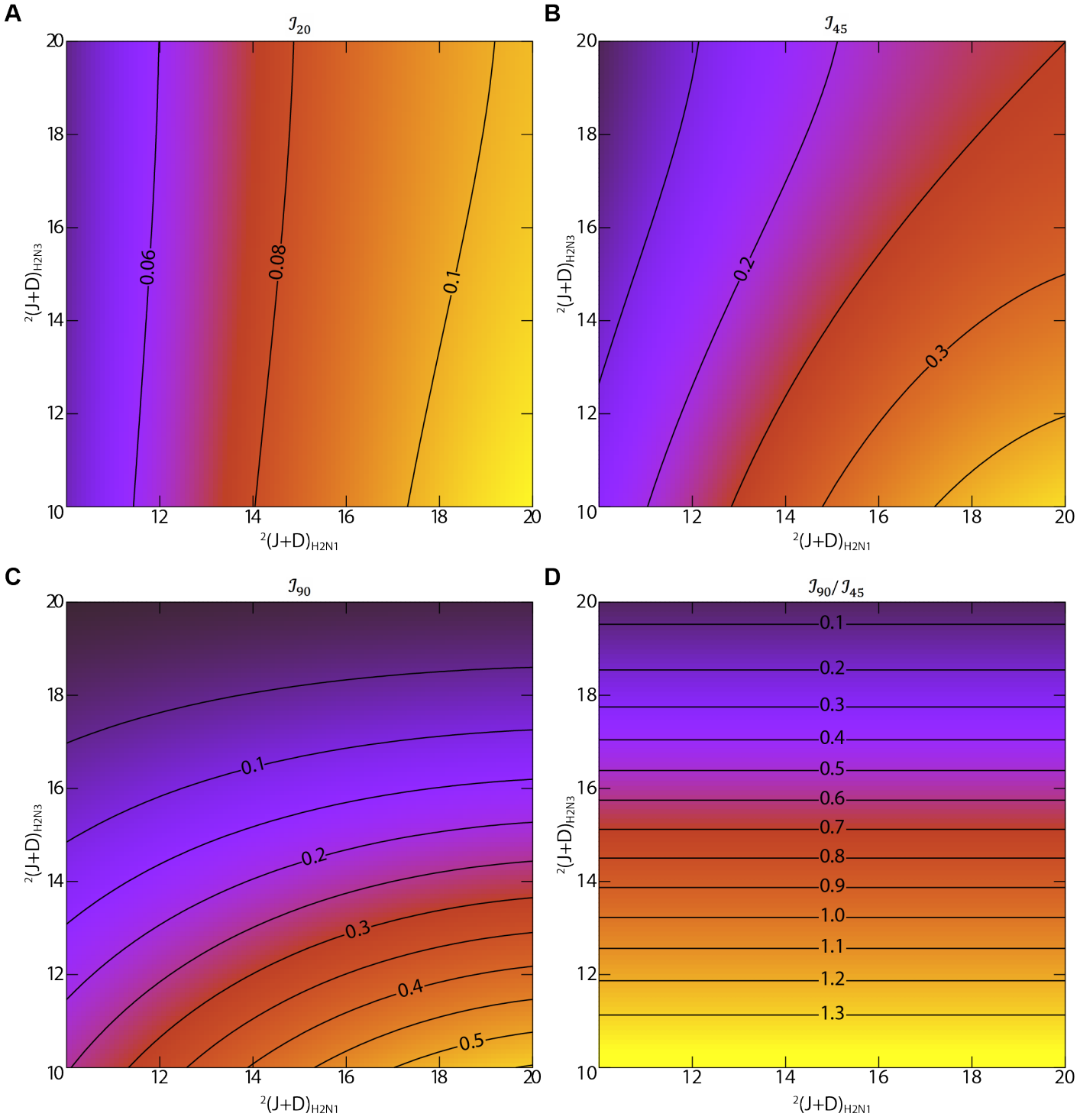

Figure S2. Intensity $\mathcal{I}_\phi$ of an HMQC signal at $(\Omega_{N1}, \Omega_{H2})$, obtained for a flip angle ϕ of the ^{15}N pulses, and de/rephasing delays of duration $1/3J$ with $J = 14.5$ Hz, where the detected H2 spin is coupled to both N1 and N3 and taking $J_{N1N3} = 0$. (A) With $\phi = 20°$ the contribution of the passive coupling to N3 is small. (B) With $\phi = 45°$ and (C) $\phi = 90°$ the contribution of the passive coupling increases. In each case the contribution of the active coupling is unchanged. (D) The contribution of the active coupling is removed by taking the ratio of two experiments where the flip angle is varied.

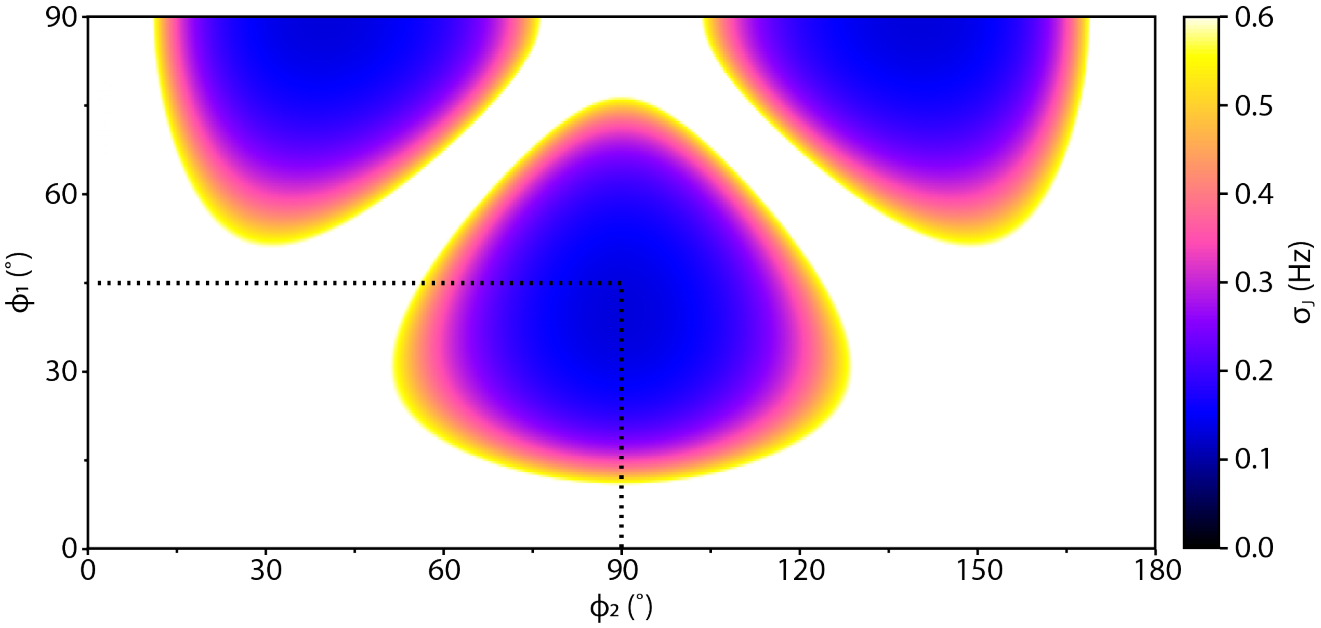

Figure S3. Uncertainty in couplings measured using the VF-HMQC approach as a function of the flip angles ϕ_1 and ϕ_2, assuming a signal to noise ratio of 50:1 with J = 15 Hz and τ = 1/3J. The flip angles giving the smallest uncertainty vary with J and τ, and are ~40° and 90° for these conditions. The work presented here uses flip angles of 45° and 90° (indicated) allowing a simple expression for the coupling in terms of the measured intensity ratio. For J = 15 Hz and τ = 1/3J the uncertainty of the coupling is expected to be 2.5% larger due to this choice.

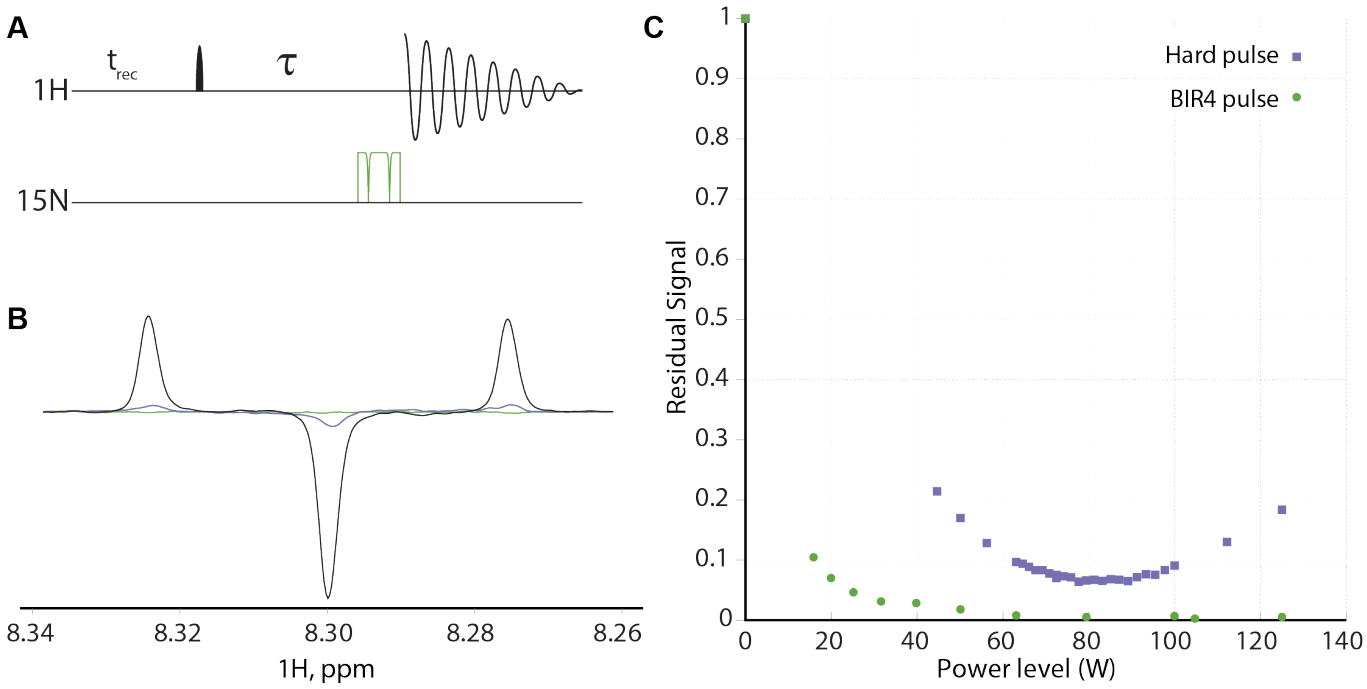

Figure S4. (A) Pulse sequence used for ^{15}N pulse calibration using U-^{15}N labeled ATP. Following excitation, antiphase $4H_yN_zN_z$ magnetization builds up during delay $\tau = 1/2J_\Sigma$, with $J_\Sigma = {}^2J_{N1H2}+{}^2J_{N1H2}$. A properly calibrated $\pi/2$ ^{15}N pulse converts this to unobservable three-spin $4H_yN_yN_y$ coherence. (B) Spectra acquired with no ^{15}N pulse (black), a carefully calibrated rectangular pulse (purple) and a BIR-4 pulse (green). Residual signal for the rectangular pulse indicates inhomogeneity across the sample. (C) Residual signal against peak power for 40 μs rectangular (purple) and 600 μs BIR-4 (green) pulses. The best calibrated rectangular pulses leave ~6.5% residual signal. No residual signal is detected for the BIR-4 pulse as long as the power is sufficiently high to meet the adiabatic condition.

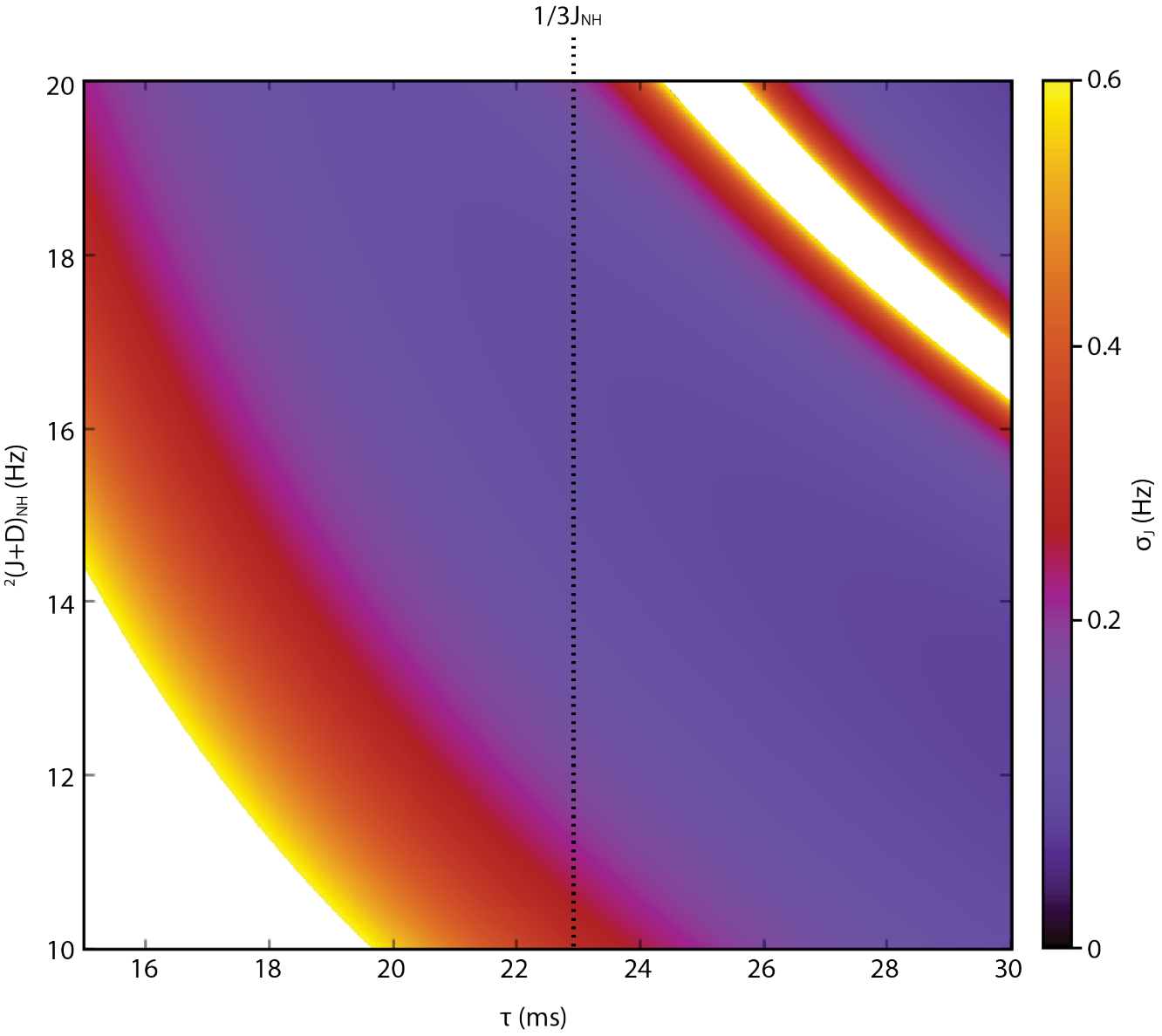

Figure S5. Uncertainty in couplings measured using the VF-HMQC approach as a function of the coupling and the de/rephasing delay τ, assuming a signal to noise ratio of 50:1 for a 15 Hz coupling with τ=1/3J.

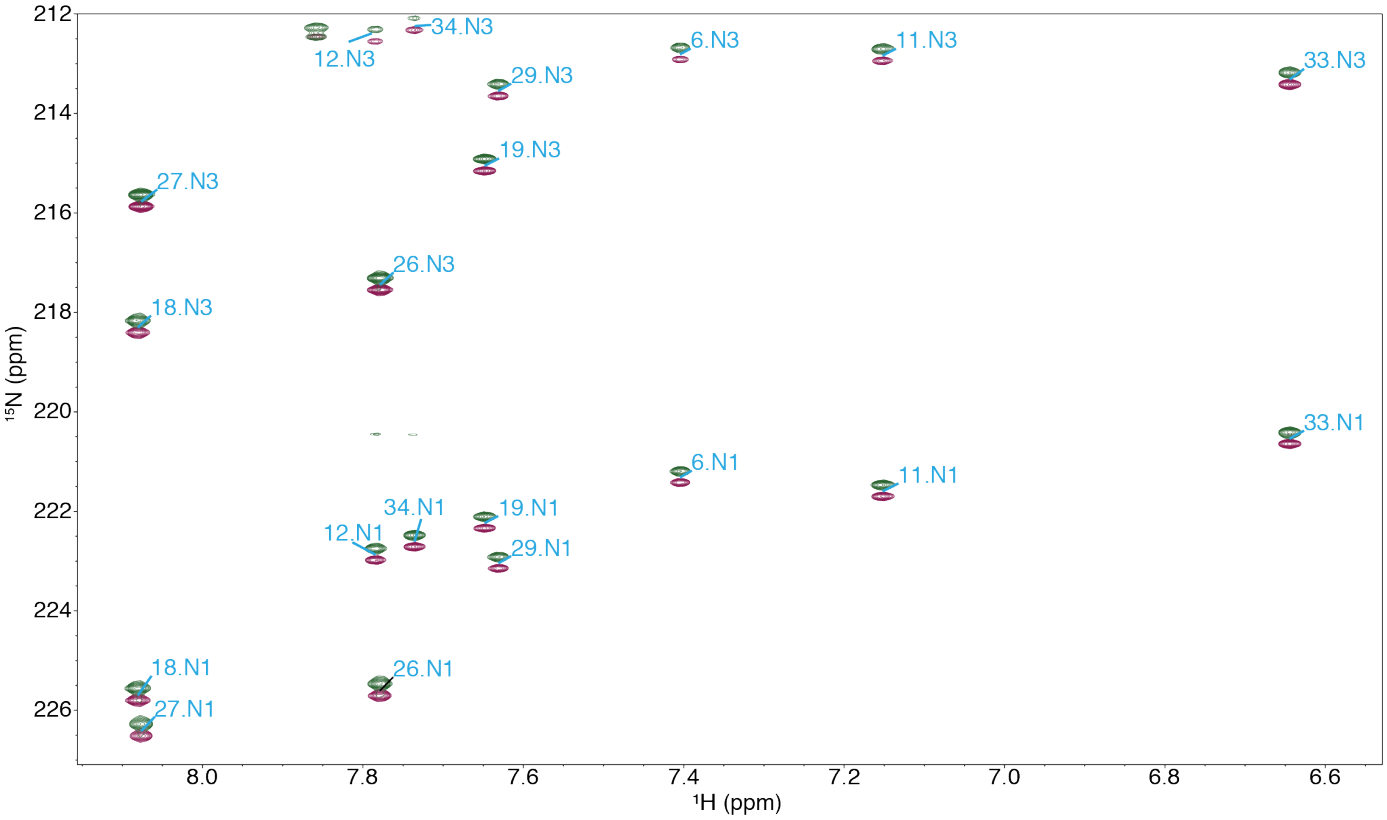

Figure S6. S^3E spectra of SLC^A recorded at 600 MHz ^{1}H frequency under isotropic conditions at 308 K, showing assignments. The spectra were recorded with 128 scans per FID, and the total matrix for the interleaved spectra comprised 2 × 256* × 1024* data points, with N* referring to N complex data points, for acquisition times of 248 ms (t_1) and 107 ms (t_2). The interscan delay was 1.5 s. The total measuring time for the two interleaved spectra was *ca.* 2 d 19 h.

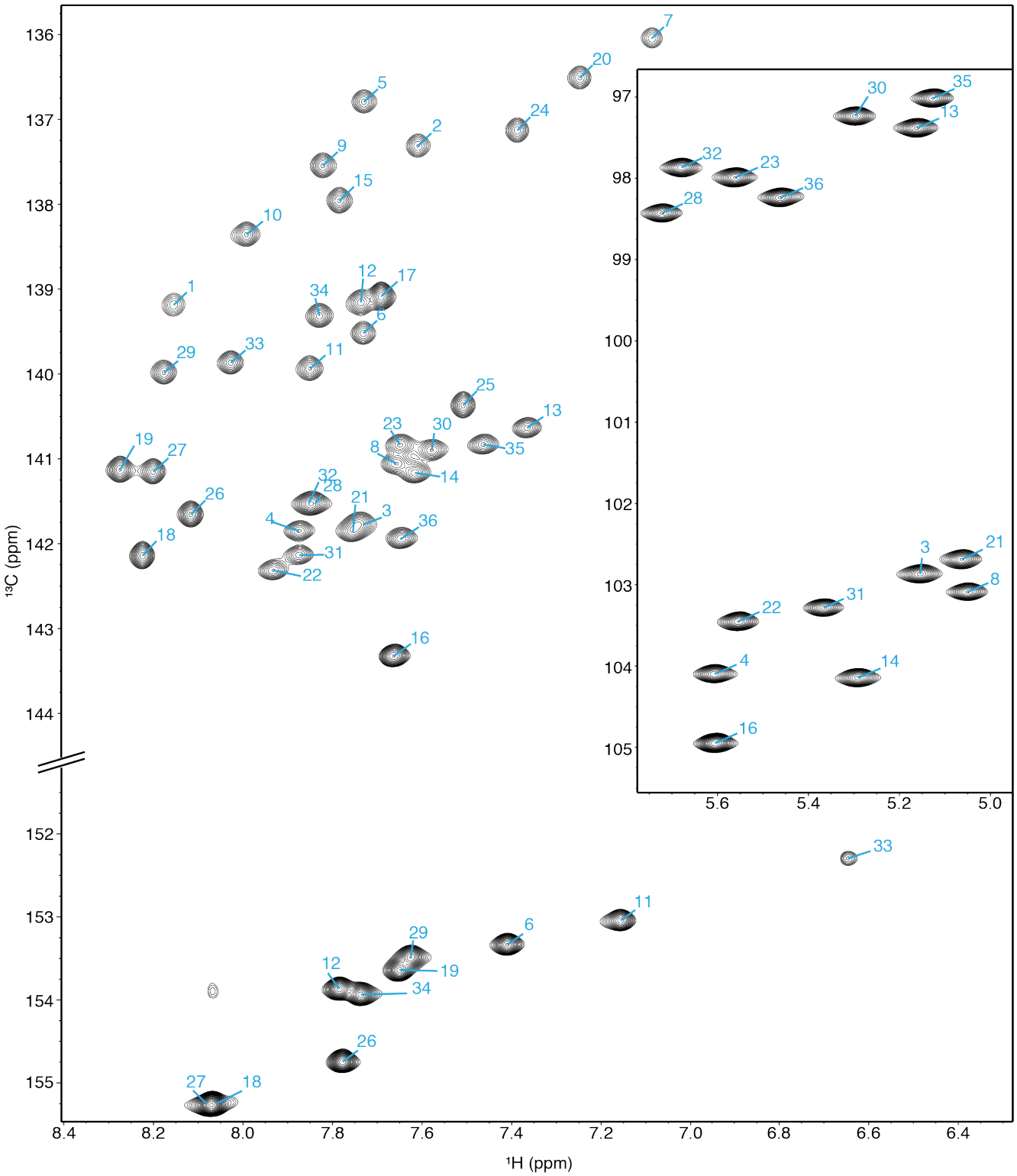

Figure S7. ARTSY reference spectra of SLC^{A} recorded at 600 MHz ^{1}H frequency under isotropic conditions at 308 K, showing residue assignments. The C-H ARTSY spectra were recorded with 16 scans per FID, and the total matrix for the interleaved reference and attenuated spectra comprised 2 × 256* × 1024* data points, with N* referring to N complex data points, for acquisition times of 81 ms (t_1) and 95 ms (t_2). The interscan delay was 3.2 s. The total measuring time for the interleaved spectra was *ca.* 16 h. The C5H5 ARTSY spectra (inset) were recorded with 8 scans per FID, and the total matrix for the interleaved spectra comprised 2 × 350* × 512* data points, for acquisition times of 101 ms (t_1) and 107 ms (t_2). The interscan delay was 3.0 s. The total measuring time for the interleaved spectra was *ca.* 10 h.

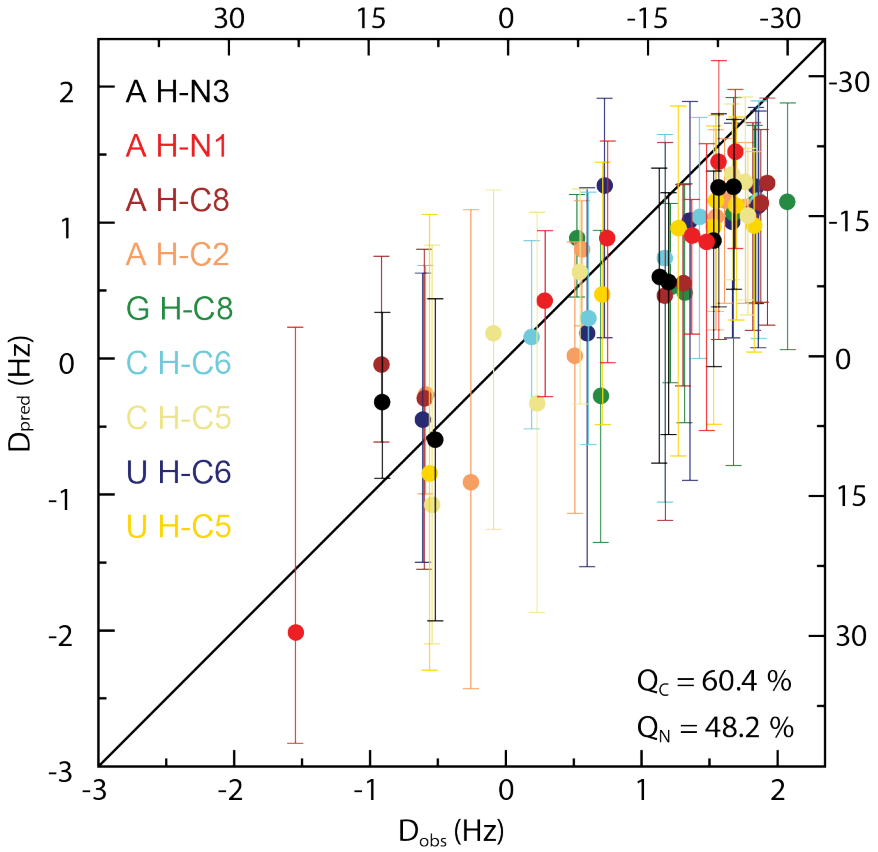

Figure S8. Observed RDCs plotted against those back-calculated for the ensemble of SLC^A models shown in Fig. 3A. The models lack the four-nucleotide GGAA bulge and were calculated using NOE restraints but not with RDC restraints. Error bars for D_{pred} represent the maximum and minimum RDCs calculated for the ensemble. ^1H-^{15}N RDCs correspond to the scales shown at the bottom and left axes. Scales for the ^1H-^{13}C RDCs are on the top and right axes.

Appendix 1

The uncertainty σ_x of a measurement x due to uncertainties σ_i in variables y_i, assuming the uncertainties are not correlated, is given by:

$$\sigma_x^2 = \sum_i \left(\frac{\delta x}{\delta y_i}\right)^2 \sigma_i^2 \tag{S1}$$

Using

$$R_S = \frac{\mathcal{I}_{45}}{\mathcal{I}_{90}} \tag{S2a}$$

$$\frac{\delta R_S}{\delta \mathcal{I}_{90}} = -\frac{\mathcal{I}_{45}}{\mathcal{I}_{90}^2} \tag{S2b}$$

$$\frac{\delta R_S}{\delta \mathcal{I}_{45}} = \frac{1}{\mathcal{I}_{90}} \tag{S2c}$$

and taking the uncertainty N for each intensity measurement to be identical for both spectra,

$$\begin{aligned}\sigma_R^2 &= \left(-\frac{\mathcal{I}_{45}}{\mathcal{I}_{90}^2}\right)^2 N^2 + \left(\frac{1}{\mathcal{I}_{90}}\right)^2 N^2 \\ &= \left(\frac{N}{\mathcal{I}_{90}}\right)^2 \left(\left(\frac{\mathcal{I}_{45}}{\mathcal{I}_{90}}\right)^2 + 1\right)\end{aligned} \tag{S2d}$$

Thus

$$\sigma_R = \frac{N\sqrt{R_S^2 + 1}}{\mathcal{I}_{90}} \tag{S3}$$

as given in **Equation 6**.

The uncertainty σ_J can similarly be found using:

$$\sigma_J^2 = \left(\frac{\delta J_{IT}}{\delta R_S}\right)^2 \sigma_R^2 \tag{S4}$$

Given

$$J_{IT} = \frac{\operatorname{atan}\left(\sqrt{4R_S - 2}\right)}{\pi\tau} \tag{S5}$$

repeated application of the chain rule yields:

$$\frac{\partial J_{IT}}{\partial R_S} = \frac{2}{\pi\tau\sqrt{4R_S - 2}(4R_S - 1)} \tag{S6}$$

And thus:

$$\begin{aligned}\sigma_J &= \left|\frac{2}{\pi\tau\sqrt{4R_S - 2}(4R_S - 1)}\sigma_R\right| \\ &= \left|\frac{2N\sqrt{R_S^2 + 1}}{\mathcal{I}_{90}\pi\tau\sqrt{4R_S - 2}(4R_S - 1)}\right|\end{aligned} \tag{S7}$$

as given in **Equation 8**.